

European soil NO_x emissions derived from satellite NO₂ observations

Xiaojuan Lin¹, Ronald J. van der A², Jos de Laat³, Vincent Huijnen², Bas Mijling⁴, Jieying Ding⁴, Henk Eskes³, John Douros³, Mengyao Liu³, Xin Zhang⁵, and Zhu Liu¹

¹Tsinghua University

²KNMI

³Royal Netherlands Meteorological Institute

⁴KNMI Royal Netherlands Meteorological Institute

⁵SRON Netherlands Institute for Space Research

December 10, 2023

Abstract

We introduce an innovative method to distinguish soil nitrogen oxides (NO_x=NO+NO₂) emissions from satellite-based total NO_x emissions using its seasonal characteristics. To evaluate the approach, we compare the deviation between the tropospheric NO₂ concentration observed by satellite and two atmospheric composition model simulations driven by the newly estimated soil NO_x emissions and the Copernicus Atmosphere Monitoring Service (CAMS) inventory. The estimated average soil NO_x emissions in Europe are 2.5 kg N ha⁻¹ yr⁻¹ in 2019, and the annual soil NO_x emissions is approximately 2.5 times larger than that of the CAMS inventory. Our method can easily be extended to other regions at middle or high latitudes with similar seasonal characteristics of soil emissions. The soil emissions are subtracted from the total NO_x emissions yielding realistic anthropogenic NO_x emissions. We further show this also yields realistic anthropogenic CO₂ emissions using known CO₂/NO_x factors from bottom-up inventories.

Hosted file

980824_0_art_file_11648901_s509hw.docx available at <https://authorea.com/users/705641/articles/691199-european-soil-nox-emissions-derived-from-satellite-no2-observations>

Hosted file

980824_0_supp_11639499_s4w9tm.docx available at <https://authorea.com/users/705641/articles/691199-european-soil-nox-emissions-derived-from-satellite-no2-observations>

European soil NO_x emissions derived from satellite NO₂ observations

Xiaojuan Lin^{1,2}, Ronald van der A², Jos de Laat², Vincent Huijnen², Bas Mijling², Jieying Ding², Henk Eskes², John Douros², Mengyao Liu², Xin Zhang³, and Zhu Liu¹

¹Department of Earth System Science, Ministry of Education Key Laboratory for Earth System Modeling, Institute for Global Change Studies, Tsinghua University, Beijing, 100084, China.

²KNMI, Royal Netherlands Meteorological Institute, De Bilt, 3730 AE, the Netherlands.

³SRON Netherlands Institute for Space Research, Leiden, 2333 CA, the Netherlands

Corresponding author: Ronald van der A and Zhu Liu (avander@knmi.nl;
zhuliu@tsinghua.edu.cn.)

Key Points:

- An innovative method is introduced to derive soil NO_x emissions in Europe from satellite NO₂ observations.
- The resulting soil NO_x emissions are at least two times larger than widely used bottom-up soil NO_x emission estimates.
- This satellite observation-based method provides a valuable independent estimate of the soil NO_x emissions.

18 **Abstract**

19 We introduce an innovative method to distinguish soil nitrogen oxides ($\text{NO}_x = \text{NO} + \text{NO}_2$)
20 emissions from satellite-based total NO_x emissions using its seasonal characteristics. To evaluate
21 the approach, we compare the deviation between the tropospheric NO_2 concentration observed
22 by satellite and two atmospheric composition model simulations driven by the newly estimated
23 soil NO_x emissions and the Copernicus Atmosphere Monitoring Service (CAMS) inventory. The
24 estimated average soil NO_x emissions in Europe are $2.5 \text{ kg N ha}^{-1} \text{ yr}^{-1}$ in 2019, and the annual
25 soil NO_x emissions is approximately 2.5 times larger than that of the CAMS inventory. Our
26 method can easily be extended to other regions at middle or high latitudes with similar seasonal
27 characteristics of soil emissions. The soil emissions are subtracted from the total NO_x emissions
28 yielding realistic anthropogenic NO_x emissions. We further show this also yields realistic
29 anthropogenic CO_2 emissions using known CO_2/NO_x factors from bottom-up inventories.

30

31 **Plain Language Summary**

32 Soil nitrogen oxide emissions ($\text{NO}_x = \text{NO} + \text{NO}_2$) are an important source of air pollution,
33 accounting for about 15% of global NO_x emissions. Unfortunately, soil emissions are not always
34 accurately described by current bottom-up inventories. Accurate quantification is beneficial for
35 clarifying the contribution of biogenic sources to air quality and developing more targeted air
36 quality measures. We present an innovative method for estimating soil NO_x emissions from
37 satellite-based total NO_x emissions. The newly estimated annual emissions in Europe are about
38 2.5 times higher than reported in previous studies. The method is evaluated by comparing the
39 deviation between the simulated and satellite observed tropospheric NO_2 concentrations. This
40 method can also be extended to other regions around the world with similar seasonal
41 characteristics of soil NO_x emissions. Anthropogenic NO_x emissions are determined by
42 subtracting the soil NO_x emissions from total NO_x emissions. We further show these
43 anthropogenic NO_x emissions can be converted into realistic CO_2 emissions by using known
44 CO_2/NO_x emission factors.

45

46 **1 Introduction**

47 Nitrogen oxides ($\text{NO}_x = \text{NO} + \text{NO}_2$) are important pollutants and their subsequent oxidation
48 products have detrimental impacts on human health and crop production (Skalska et al., 2010).
49 Soil NO_x emissions are the largest contributor to the NO_x budget besides combustion sources,
50 contributing up to ~15% of global NO_x emissions (Hudman *et al.*, 2012; Vinken et al., 2014;
51 Weng et al., 2020). The relative contribution of soil NO_x to total NO_x emissions is gradually
52 increasing due to steadily declining anthropogenic NO_x emissions as a result of successful
53 emission reduction strategies in, e.g., China (van der A et al., 2017; Lu et al., 2021), the USA
54 (Zhang et al., 2003; Silvern et al., 2019), and Europe (Rafaj et al., 2015; Skiba et al., 2020).
55 Furthermore, soil NO_x emissions play a non-negligible role in rural air pollution especially
56 during summer time while fossil fuel combustion emissions are relatively constant over the year
57 (Fortems-Cheiney et al., 2021; Wang et al., 2022). The precise quantification of soil NO_x
58 emissions is therefore essential for assessing emission control strategies and a better
59 understanding of air quality.

60 Two microbial processes, nitrification and denitrification, are the main sources of soil NO_x and
61 they occur in agricultural and natural ecosystems (Hall et al., 1996; Pilegaard, 2013). Key factors
62 that regulate NO_x emissions from soil are: temperature, soil moisture and texture, soil pH,
63 nutrient availability, ecosystem types, agricultural management and ambient atmospheric NO_x
64 concentration (Hall et al., 1996; Butterbach-Bahl et al., 2013; Medinets et al., 2015). Chamber
65 studies and field measurements are commonly employed to investigate the response of soil NO_x
66 emissions to rewetting of dry soils (Garcia-Montiel et al., 2003; Hickman et al., 2021), fertilizer-
67 induced change (Liu et al., 2017; Song et al., 2020; Hui et al., 2023) and atmospheric deposition
68 (Hall and Matson, 1999; Venterea et al., 2003; Koehler et al., 2009; Eickenscheidt and Brumme,
69 2012). Global and regional soil NO_x emissions are generally estimated by three different model-
70 based methods: simple scaling (Davidson and Kingler, 1997), empirical models (Yienger and
71 Levy II, 1995; Yan et al., 2005; Weng et al., 2020; Simpson and Darras, 2021) and process-
72 oriented models (Butterbach-Bahl et al., 2009; Molina-Herrera et al., 2017). However, these
73 models in general disagree about the soil NO_x quantities and their spatial patterns.

74 Satellite-based observations provide an alternative method to derive soil NO_x emissions. Bertram
75 et al. (2005) and Zörner et al. (2016) found that SCIAMACHY (Scanning Imaging Absorption
76 spectroMeter for Atmospheric CHartographY) observations captured the brief, high-intensity soil
77 NO_x pulses in response to fertilizer application or rainfall events in agricultural regions and semi-
78 arid ecosystems. Other studies constrained soil NO_x emissions top-down using retrieved NO_2
79 vertical column densities (VCDs) from the Ozone Monitoring Instrument (OMI) for East China
80 (Lin, 2012) and globally (Vinken et al., 2014). Huber *et al.* (2020) used the unprecedented
81 spatiotemporal resolution of the TROPOMI NO_2 product to quantify soil-driven contributions of
82 cropland to regional NO_x emissions by a box model on daily to seasonal scales for the U.S.
83 Southern Mississippi River Valley. Furthermore, other studies estimate NO_x emissions by
84 analyzing the relationship between observed NO_2 concentrations and NO_x emissions with
85 inversion techniques that consider the transport process of NO_x (Mijling and van der A, 2012;
86 Miyazaki et al., 2012). However, such methods estimate only total NO_x emissions, encompassing
87 both natural and anthropogenic sources.

88 In this study, we introduce a new method for estimating soil NO_x emissions in individual grid
89 cells based on its seasonal variations. This method is a post-processing of the total NO_x
90 emissions derived by the inverse algorithm DECSO (Daily Emission estimation Constrained by
91 Satellite Observations, Mijling and van der A, 2012; Ding et al., 2017a) applied to NO_2
92 observations over Europe by TROPospheric Monitoring Instrument (TROPOMI) on Sentinel 5
93 Precursor (S5-P) satellite. We evaluate the performance of our method by comparing the
94 deviation of the tropospheric NO_2 concentrations between atmospheric chemistry model
95 simulations and observations by TROPOMI. Finally, we explore the potential to use the
96 difference between total satellite-derived NO_x emissions and soil NO_x emissions for indirectly
97 estimating fossil-fuel CO_2 emissions.

98 **2 Materials and Methods**

99 **2.1 NO_x emissions from DECSO**

100 NO_x emissions are derived by the state-of-the-art inverse algorithm DECSO (Daily Emission
101 estimation Constrained by Satellite Observations, Mijling and van der A, 2012; Ding et al.,
102 2017a). DECSO is specifically developed for daily updates of emissions of short-lived

103 atmospheric constituents using satellite observations. The algorithm solves the sensitivity of
 104 concentrations to emissions using a single forward run of the chemical transport model
 105 CHIMERE v2020 (Menut et al., 2021) and a simplified 2D trajectory analysis. An extended
 106 Kalman filter is used for assimilation of the observed column concentrations in the inversion step.
 107 DECSO is able to provide total emissions from biogenic (originating from soil for NO_x) and
 108 anthropogenic sources for short-lived chemical species and it can detect new emission sources
 109 that may be missing in bottom-up inventories. It has been validated (Ding et al., 2017b) and
 110 successfully applied to different regions using OMI and TROPOMI observations (Ding et al.,
 111 2015; Ding et al., 2018; Ding et al., 2020; van der A et al., 2020; Ding et al., 2022). In this study,
 112 monthly NO_x emissions in 2019 over Europe (10°W-30°E, 35-55°N) are derived from
 113 TROPOMI NO₂ observations using DECSO on a spatial resolution of 0.2° × 0.2°. These total
 114 emissions are used as input to isolate soil NO_x emissions in a post-processing step, which is
 115 explained below.

116 2.2 Soil NO_x emissions estimates

117 Several studies have shown that soil NO_x emissions are significantly influenced by land use type
 118 (Valente and Thornton, 1993; Verchot et al., 1999; Yan et al., 2005). The soil emissions in our
 119 study area originate from four main land use types: forest, croplands, shrub and grassland (Figure
 120 S1). Here we merged shrub and grassland into one category (called “other biogenic”) considering
 121 their limited occurrence in the study area (Table S1c).

122 We use the following five steps (see flow chart in Figure S2) to separate soil NO_x emissions
 123 from total NO_x emissions:

124 (1) We select pixels dominated by the biogenic sector using the proportion of each land use type.
 125 The minimum thresholds of the three land use ratios (forest, crop, and other biogenic sources)
 126 are set to 0.5 for individual grid cells to make sure the cell is dominated by one of the biogenic
 127 source sector types. For these pixels, the fraction of urban coverage is required to be less than
 128 0.02 to eliminate the interference of anthropogenic emissions as much as possible. The selected
 129 pixels are referred to as biogenic pixels.

130 (2) To exclude the remaining anthropogenic emissions in the selected grid cells, we subtract
 131 CAMS anthropogenic NO_x emissions (version 5.3, called CAMS-ant) from the DECSO total
 132 NO_x emissions. Note that this is only done for the selected biogenic pixels. If negative values
 133 occur after subtraction, they are set to zero. A sensitivity analysis with respect to this step is
 134 described in Section 3.1.

135 (3) In order to better reflect the spatial heterogeneity of soil emissions, we divide the research
 136 area equally into 5 subregions in the latitude direction by 2 subregions in the longitude direction.
 137 In each of these 10 subregions, the average monthly emissions of the selected pixels are fitted

138 with a Gaussian function $f(x) = A e^{-\frac{(x-B)^2}{2C^2}}$ over one year. We chose a Gaussian function as soil
 139 NO_x emissions in Europe vary slowly with season with typically a winter minimum and summer
 140 maximum. The fitting parameters A , B , and C are obtained for pixels dominated by each of the
 141 land use types separately (see step 1). A represents the maximum soil NO_x emissions in a year, B
 142 represents the month when the maximum soil emissions occur, and C determines the width of the
 143 Gaussian curve and thus the length of the season, which also affects the amount of winter soil
 144 NO_x emissions. Examples of the Gaussian fitting can be found in Figure S3.

145 (4) Since the parameters obtained in step 3 represent soil emissions with a specific land use ratio
146 larger than 0.5 (set in step 1) but still with mixed land use types, we use the solution of formula
147 S2 to obtain the typical parameters of pure pixels, *i.e.* the land use ratio of one of the three types,
148 either forest, crop, or other biogenic sources, equals 1. In this way, we obtain 30 sets of
149 parameters (*A*, *B*, and *C*) representing soil emissions for three land-use types and 10 subregions
150 separately. To smooth the transitions between subregions, we perform a two-dimensional
151 interpolation to obtain the parameters for each land-use type and for each grid cell separately.

152 (5) We assume that the land use ratio directly determines the proportion of soil NO_x emissions.
153 The monthly soil emissions per grid cell is calculated by multiplying the ratio of the three land
154 use types by the three Gaussian functions of the corresponding soil emission types, and adding
155 them together.

156 (6) If the soil emission calculated at a certain grid cell is larger than the total emission of DECSO
157 in a certain month, the soil emission of this month is set to be equal to this total emission of
158 DECSO. In this way the total of the derived DECSO emissions remain conserved. The end
159 product will be called DECSO-soil from here.

160 Figure S4 shows the three key parameters *A*, *B*, and *C* that depict the seasonal characteristics of
161 soil NO_x emissions for the three different land use types, with significant zonal and meridional
162 differentiation. The value of parameter *A*, representing the maximum soil NO_x emissions during
163 the year, for forests and croplands are generally similar (Figure S4 a-c). The month of the
164 maximum soil emissions (parameter *B*) occurs a bit later in forest areas (July - August) than in
165 croplands areas (June - July) (see Figure S4 d-f). The parameter *C* represents the width of the
166 Gaussian fit and this also affects winter soil NO_x emissions. For all three land use types,
167 parameter *C* shows a clear decreasing trend with increasing latitude (Figure S4 g-i). This is
168 because the higher the latitude, the lower the winter temperature, and the lower the microbial
169 activity, resulting in a shorter active season.

170 2.3 Emission inventories and land use dataset

171 In this study, three emission inventories are used for comparison with our estimates. They are the
172 CAMS soil emissions inventory (CAMS-GLOB-SOIL version 2.4, henceforth called CAMS-
173 soil), the Harvard-NASA Emissions Component (HEMCO) soil emissions inventory (version
174 2021, called HEMCO-soil) and the National Long-range Transboundary Air Pollution (LRTAP)
175 NO_x emissions (called LRTAP-NO_x). CAMS-soil provides gridded global monthly soil NO
176 emissions as total values and for separate source sectors at spatial resolution of 0.5°×0.5°. It is
177 based on empirical formulas and process parameter models (Simpson and Darras, 2021).
178 HEMCO-soil provides global hourly soil NO_x emissions at a horizontal resolution of 0.25° lat. ×
179 0.3125° lon. (Weng et al., 2020), (Keller et al., 2014). LRTAP-NO_x provide country level yearly
180 NO_x emissions for agriculture and other sectors and is provided by the European Environment
181 Agency. Global monthly bottom-up anthropogenic NO_x (version 5.3, called CAMS-ant) and CO₂
182 emissions (version 4.2, called CAMS-CO₂) inventories are both obtained from the Copernicus
183 Atmosphere Monitoring Service (CAMS) at a 0.1°×0.1° horizontal resolution (Soulie et al.,
184 2023). All emission data are for 2019 and are regridded to the same domain and resolution of
185 DECSO (0.2° × 0.2°). The land use data Land Cover are obtained from the Copernicus Global
186 Land Service (version3.0.1, Buchhorn et al., 2020). The original 23 land use classes of the Land
187 Cover database were first grouped into 8 new main classes, comprising ocean, urban, cropland,

188 grassland, bare land, inland water, forest, and shrub defined in Table S1. The land use ratio for
189 each class was calculated by re-gridding the original 100m resolution Land Cover product to the
190 DECSO grid of 0.2°.

191 2.4 Evaluation of derived soil emissions by comparing modelled concentrations to satellite 192 observations

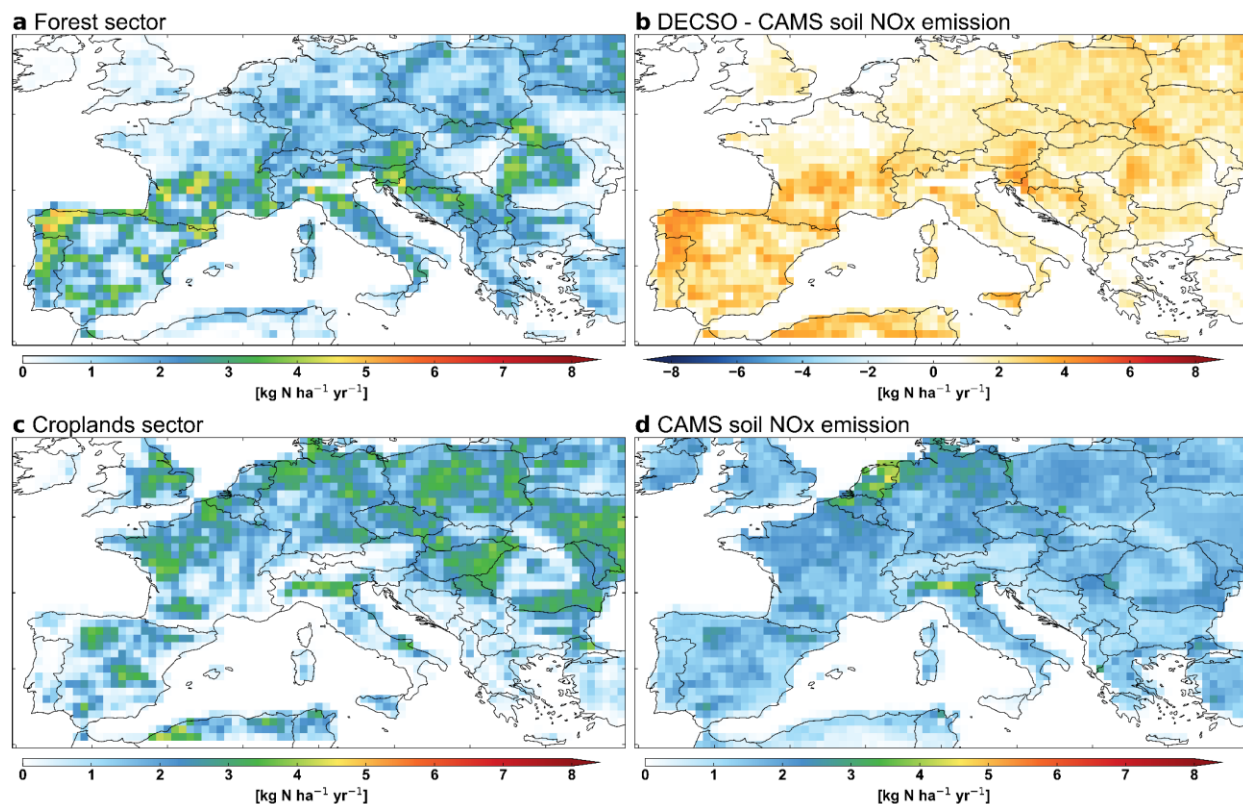
193 We conduct two comparative experiments to simulate tropospheric NO₂ columns, which use
194 either CAMS soil emissions or DECSO soil emissions. We evaluate the performance of the
195 newly estimated soil emissions in this study by comparing the Root Mean Square Error (RMSE)
196 between the simulated tropospheric NO₂ concentration and the TROPOMI observed tropospheric
197 NO₂ concentration of these two comparative experiments). The tropospheric NO₂ columns were
198 simulated by an extended version of ECMWF's Integrated Forecasting System (IFS) called "IFS-
199 COMPO" (Flemming et al., 2015; Huijnen et al., 2019). IFS-COMPO is part of the global
200 component of the Copernicus Atmosphere Monitoring Service (CAMS) and has been employed
201 to supply global analyses and forecasts of atmospheric composition in an operational mode
202 starting from 2014. The version of IFS-COMPO employed here is based on IFS CY48R1
203 (ECMWF, 2023), but with only tropospheric chemistry activated. Its default anthropogenic
204 emissions, based on CAMS-GLOB-ANT v5.3 (Soulie et al., 2023) are adopted. The model is
205 driven by our newly estimated soil NO_x emissions, and CAMS soil NO_x emissions (version 2.4,
206 Simpson and Darras, 2021) for reference. IFS-COMPO was run for the year 2019 at a horizontal
207 resolution of approximately 40 km with 137 vertical layers and 900s time steps and with a one-
208 month spin up period. When we compare TROPOMI NO₂ observations with the IFS-COMPO
209 simulation, only observations with a quality flag above 0.75 are used to avoid retrievals for
210 ground pixels covered with snow, ice or high cloud radiance fraction, as well as problematic
211 retrievals. The model outputs are interpolated to the local overpass time of TROPOMI and the
212 averaging kernel is applied to the modelled NO₂ profile. The collocated observation-model pairs
213 are re-gridded to a regular latitude–longitude grid with a 0.25° resolution using an area-weighted
214 averaging considering the area of the TROPOMI-pixel if the coverage of the grid cell is above
215 50% (Douros et al., 2023). The only difference between the two comparative model experiments
216 is the input of soil NO_x emissions.

217 **3 Results**

218 3.1 Comparison of Soil NO_x emissions with CAMS

219 Figure 1 shows the spatial distribution of calculated soil NO_x emissions for each sector (forests
220 and croplands sectors) in the study area during summer (May–August). The yearly averaged soil
221 NO_x emissions for the entire domain from forests, croplands, and other biological sources are 2.6,
222 2.6 and 2.0 kg N ha⁻¹ yr⁻¹ respectively (in May–August shown in Figure 1 they are on average 3.7,
223 3.6 and 2.9 kg N ha⁻¹ yr⁻¹), which fall within the estimated range of forest emissions (0.35 to 15.9
224 kg N ha⁻¹ yr⁻¹ in Saxony of Germany; Molina-Herrera et al. 2017) and are of the same order of
225 magnitude for croplands as estimated by Yan et al. (1.08 kg N ha⁻¹ yr⁻¹ globally; 2005). Regions
226 with high CAMS-soil emissions, such as the Castile-León plain in Spain and the Po River plain
227 in Italy, display strong similarities with the spatial distribution of DECSO-soil NO_x emissions of
228 the croplands sector (Figure 1 c-d). Furthermore, the CAMS soil NO_x emission inventory has
229 very low emissions in forest areas resulting in lower emission estimates in the northwestern
230 Iberian Peninsula, the forest areas of Romania and the south-central France (Figure 1 a-d). Note

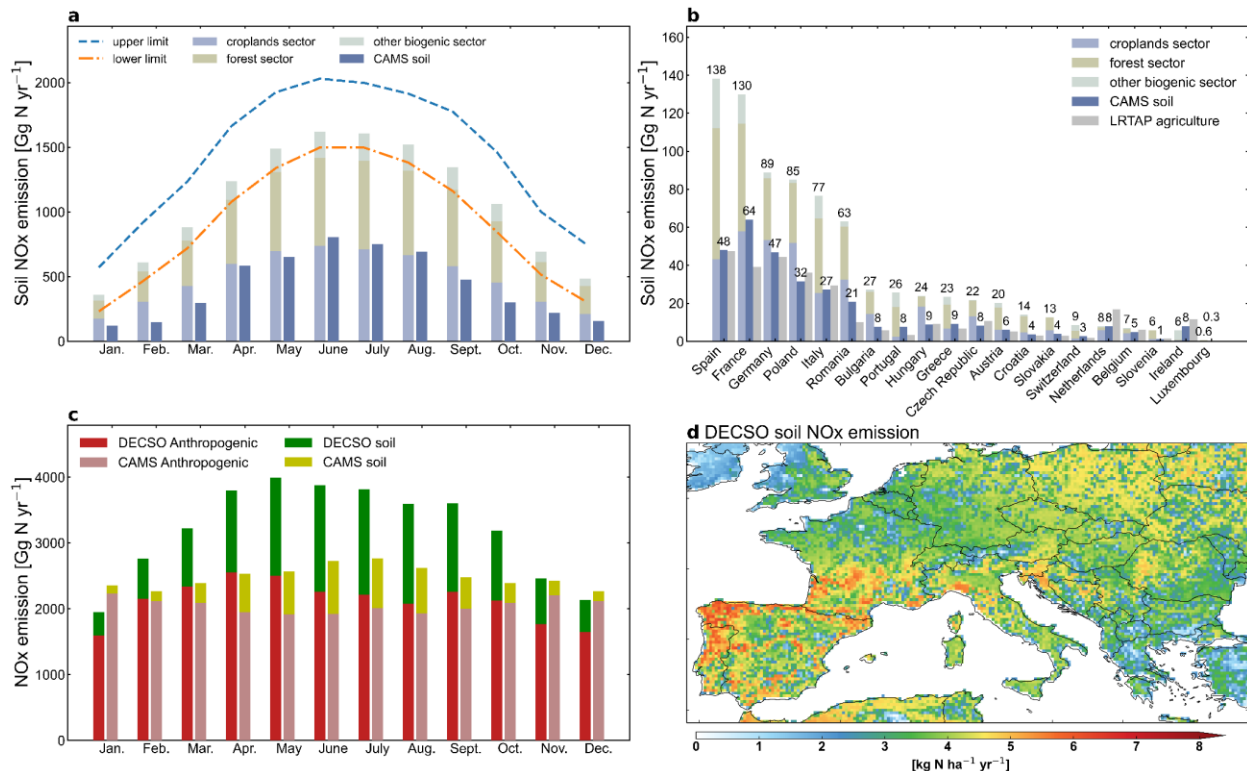
231 the high correlation ($R^2 = 0.53$ in Figure S6) between the DECSO forest emissions (Figure 1a)
 232 and the difference map shown in Figure 1b.



233
 234 **Figure 1.** The spatial distribution of the derived soil NO_x emissions during summer represented
 235 by the average emissions from May to August in 2019 from (a) forest and (c) croplands. (d)
 236 shows the CAMS-soil NO_x emissions in Europe during summer. The difference between CAMS-
 237 soil and DECSO-soil is shown in (b). The soil emissions calculated from DECSO total emissions
 238 are regridded to the resolution of CAMS-soil, which is $0.5^\circ \times 0.5^\circ$.

239 We compared the sum of all DECSO soil to sum of all CAMS soil emissions in our study
 240 domain. Our derived total annual soil NO_x emissions are 1.1 Tg N yr^{-1} , which is more than 2.5
 241 times larger than the total of CAMS-soil (0.4 Tg N yr^{-1}) and about 2.3 times higher than
 242 HEMCO (0.5 Tg N yr^{-1}) (Figure S7). The average soil NO_x emissions in the study area are 2.5 kg
 243 $\text{N ha}^{-1} \text{ yr}^{-1}$ in 2019. Figure 2a shows that the obtained typical monthly time profile of soil NO_x
 244 emissions is similar to that of CAMS. The spatial distribution and the amount of the DECSO
 245 cropland emissions are comparable to the CAMS soil emissions. CAMS-soil and LRTAP NO_x
 246 emissions from agriculture sector are also consistent for national total numbers (Figure 2b).
 247 Furthermore, we found that the discrepancy with CAMS is more significant in countries with a
 248 large proportion of forest area, such as the Spain (138 Gg N yr^{-1} for DECSO-soil and 48 Gg N yr^{-1}
 249 yr^{-1} for CAMS-soil) and France (130 Gg N yr^{-1} for DECSO-soil and 64 Gg N yr^{-1} for CAMS-soil).
 250 And the deviation is smaller in countries with a large proportion of non-forest area (Figure 2b),
 251 such as the Netherlands (about 8 Gg N yr^{-1} for both DECSO-soil and CAMS-soil) and Belgium
 252 (7 Gg N yr^{-1} for DECSO-soil and 5 Gg N yr^{-1} for CAMS-soil). Figures 2c and S8 show that after
 253 excluding soil emissions, the difference between anthropogenic NO_x emissions derived with
 254 DECSO based on satellite observations and CAMS anthropogenic emissions becomes noticeably

255 smaller (DECSO anthropogenic NO_x is 4.9 kg N ha⁻¹ yr⁻¹ and CAMS-anthropogenic is 4.8 kg N
 256 ha⁻¹ yr⁻¹).



257
 258 **Figure 2.** (a) Monthly comparison of derived soil NO_x emissions for three land use types with
 259 CAMS-soil. The estimated upper limit and the lower limit of emissions as described in below are
 260 shown by the dashed line. (b) National soil NO_x emissions from DECSO-soil and CAMS-soil.
 261 (c) The monthly proportion of anthropogenic and soil NO_x emissions of DECSO and CAMS.
 262 (d) The spatial distributions of DECSO-soil emissions in 2019 during summer (May to August).

263 3.2 Uncertainty analysis

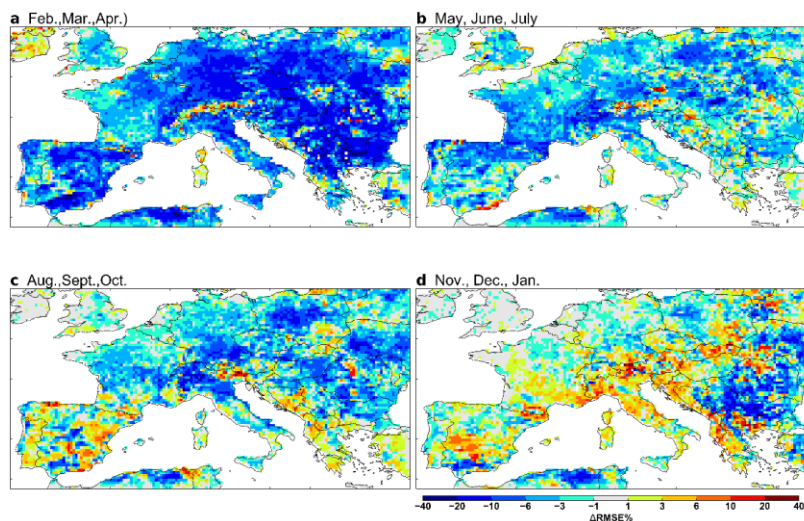
264 The biggest uncertainty in our method is caused by the correction for anthropogenic emissions in
 265 the selected biogenic grid cells (step 2 in Section 2.2). Therefore, we estimated the upper and
 266 lower limit of the calculated soil emissions, by performing a sensitivity test. We first assume all
 267 selected biogenic grid cells are without remaining anthropogenic emissions, resulting in an upper
 268 limit of the derived soil emissions. On the other hand, the lower limit of emissions is obtained by
 269 assuming that the emissions of the selected biogenic grid cells are completely anthropogenic in
 270 wintertime as biogenic activity is at a minimum in Europe during winter. Thus we replaced the
 271 anthropogenic emissions of CAMS (used in step 2 of Section 2.2) by the average of the DECSO
 272 total emissions in January and December. This results in an upper limit of about 33% higher
 273 emissions and a lower limit that is about 14% lower than the calculated DECSO-soil emissions
 274 (Figure S5).

275 The derived soil NO_x emissions are sensitive to uncertainties in the derived DECSO emissions.
 276 The DECSO emissions have a precision of about 30% for monthly emissions in a single grid cell.
 277 However, for this analysis on average soil emissions, the DECSO emissions are averaged over
 278 pixels over the whole region and thus strongly reduced compared to single grid cells. Therefore,

279 the error of the anthropogenic emission correction mentioned above is dominating, and we
 280 estimate the uncertainty on the average soil emissions to be about 30%.

281 3.3 Assessment of the DECSO soil emissions using IFS-COMPO simulations

282 Figure 3 shows the change of RMSE (Δ RMSE%) between the TROPOMI observations and the
 283 simulated tropospheric NO₂ concentration in the IFS-COMPO model driven by the DECSO-soil
 284 and CAMS-soil emissions. The smaller the deviation, the higher the reliability of the soil
 285 emissions compared to TROPOMI. Figure 3a-d shows the spatial distribution and seasonal
 286 variation of Δ RMSE% calculated by formula S3. A negative Δ RMSE% represents that the model
 287 simulation deviation driven by DECSO-soil is smaller than that driven by CAMS-soil, meaning
 288 that the DECSO-soil are more consistent with TROPOMI observations than that of CAMS-soil.
 289 While we use the same TROPOMI NO₂ observations as employed in the DECSO optimization
 290 procedure, the atmospheric composition modeling framework is fully independent to DECSO.
 291 We found that simulations driven by DECSO soil emissions performed significantly better than
 292 using CAMS soil over most of Eastern Europe, North Africa, and Spain (blue area in Figure 3),
 293 especially in spring and autumn (Figure S9), when the percentual emissions changes with respect
 294 to CAMS-Soil are largest. The spatial distribution of changes in Δ RMSE% in areas dominated
 295 by rural area, forest, and croplands area is shown in Figure S10-S12. Overall, the simulated
 296 RMSE% of DECSO soil is lower than that of CAMS soil, about 6% lower in spring and 2%
 297 lower in autumn (Figure S9). In general, the newly calculated soil emissions significantly reduce
 298 the error of the simulated and observed tropospheric NO₂ concentrations, which shows the
 299 consistency of the DECSO-soil. The negative Δ RMSE% over forest shows that soil NO_x
 300 emissions over forest are underestimated by CAMS.

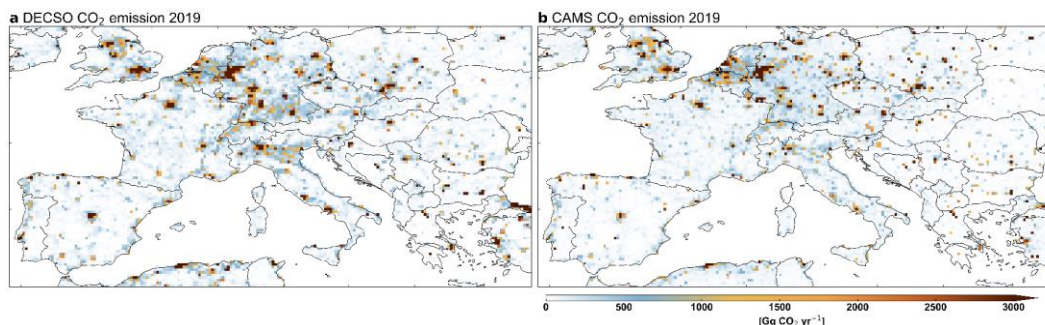


301
 302 **Figure 3.** The deviation of observed and simulated tropospheric NO₂ concentrations driven by
 303 DECSO-soil and CAMS-soil (a-d) represented by Δ RMSE%. The average of Δ RMSE% in (a)
 304 spring, (b) summer, (c) autumn and (d) winter calculated by formula S3. RMSE refers to the
 305 average difference between the simulated tropospheric NO₂ concentration and the observed
 306 tropospheric NO₂ concentration. Subtracting RMSE of experiment 2 from that of experiment 1
 307 yields Δ RMSE. Dividing Δ RMSE by the average of the simulated tropospheric NO₂
 308 concentration results of the two experiments results in Δ RMSE%. A negative Δ RMSE% shown

309 in blue means that the DECSO-soil are more consistent with TROPOMI observations than that of
 310 CAMS-soil.

311 3.4 Indirect estimates of anthropogenic CO₂ emissions

312 Since anthropogenic NO_x and CO₂ emissions are usually released simultaneously, several studies
 313 have used the NO_x emissions retrieved from satellite observations to infer the anthropogenic CO₂
 314 emissions of countries or regions by a top-down method (de Laat and van der A, 2019; Zheng et
 315 al., 2020; Li et al., 2023; Miyazaki and Bowman, 2023). However, these studies did not consider
 316 the fact that the NO_x emissions retrieved based on satellite observations include non-
 317 anthropogenic soil NO_x emissions. After subtracting soil NO_x emissions from the total NO_x of
 318 DECSO, we can calculate the co-emitted CO₂ emissions by multiplying DECSO anthropogenic
 319 NO_x emissions with the NO_x/CO₂ emission factors obtained from CAMS inventory. The spatial
 320 pattern of CO₂ emissions based on DECSO has a high overall consistency with the bottom-up
 321 CAMS emission inventory (Figure 4). The annual CO₂ emissions derived from DECSO (called
 322 DECSO-CO₂) in the study area in 2019 is 3.7 Gt, which is comparable with the 3.2 Gt of the
 323 CAMS inventory (called CAMS-CO₂). Overall, this reflects the potential of using DECSO to
 324 indirectly infer fossil-fuel CO₂ emissions, especially for regions where CO₂ emissions are less
 325 well-known than in Europe.



326
 327 **Figure 4.** The spatial distributions of (a) estimated annual CO₂ emissions using DECSO, and (b)
 328 bottom-up CO₂ emission inventory CAMS.

329 4 Conclusions

330 We have developed a method for estimating soil NO_x emissions based on their seasonal
 331 characteristics, which we derive from the non-urban regions in our study domain, in our case
 332 Europe. The method starts from satellite-based total NO_x emissions derived with the DECSO
 333 emission inversion system. The estimated soil NO_x emissions based on DECSO is 2.5 kg N ha⁻¹
 334 yr⁻¹ for Europe in 2019. We found that the existing widely used soil NO_x emission inventories
 335 CAMS and HEMCO (based on empirical and statistical models) report lower soil NO_x emissions
 336 by about 2.5 times. To assess the reliability of the derived DECSO soil NO_x emissions, we tested
 337 them using IFS-COMPO simulations. The model-simulated tropospheric NO₂ concentrations
 338 driven by DECSO soil NO_x are closer to the NO₂ concentrations observed by TROPOMI than
 339 the simulation driven by CAMS soil emissions. The improvement was especially observed in
 340 spring, with a RMSE% reduction of 6%. When checking the spatial distribution (Fig.2), it seems
 341 that the discrepancy originates mainly from the forests, where the DECSO derived soil emissions
 342 are much higher than those in the CAMS inventory. Possibly the soil NO_x emissions from forests

343 in Europe are currently underestimated. Not many studies are yet performed to European forest
344 emissions, but Molina-Herrera et al. (2017) concluded that for the state of State of Saxony,
345 Germany both agricultural and forest area are significant sources of soil NO_x .

346 The seasonal characteristic of DECSO-soil is consistent with the European regional soil NO_x
347 emissions calculated by Simpson and Darras (2021) based on empirical formulas and process
348 parameter models (see Figure S13b). Regions with similar seasonal patterns of soil NO_x
349 emissions as the European region are found at mid-latitudes including North America, North
350 Africa, East Asia, Russia (Figure S13 from Simpson and Darras, 2021) making these regions
351 suitable for deriving soil NO_x emissions from satellite with the same approach. For mid-latitude
352 regions in the southern hemisphere such as Australia, this method can also be used by shifting
353 the peak parameter to wintertime.

354 Our method exploits observations from satellites for a better understanding of the amount and
355 spatiotemporal variation of soil NO_x emissions. The method, starting from DECSO total
356 emissions, is computationally fast and regionally consistent. After isolating the contribution of
357 soil NO_x, the remainder can be attributed to anthropogenic emissions and the total amount and
358 spatial patterns of anthropogenic CO₂ emissions can be indirectly estimated. The results for
359 Europe are consistent with the bottom-up CO₂ inventory, which demonstrate the potential for
360 DECSO to expand its application to other regions in the world with less information on CO₂
361 emissions.

362

363

364

365 **Acknowledgments**

366 This research has been supported by the project “Sentinel EO-based Emission and Deposition
367 Service” of the European Union's Horizon 2020 research and innovation programme (SEEDS,
368 grant number 101004318). The support provided by the China Scholarship Council (CSC) during
369 a visit by Xiaojuan Lin to the Royal Netherlands Meteorological Institute (KNMI) is
370 acknowledged.

371

372 **Open Research**

373 TROPOMI data is available at: <https://www.tropomi.eu/data-products/nitrogen-dioxide>. CAMS soil

374 NO_x emissions are available at: <https://permalink.aeris-data.fr/CAMS-GLOB-SOIL>. HEMCO soil NO_x

375 emissions are available at: [https://figshare.com/articles/dataset/Global_high-](https://figshare.com/articles/dataset/Global_high-resolution_emissions_of_soil_NOx_sea_salt_aerosols_and_biogenic_VOCs/9962216/4)

376 [resolution_emissions_of_soil_NOx_sea_salt_aerosols_and_biogenic_VOCs/9962216/4](https://figshare.com/articles/dataset/Global_high-resolution_emissions_of_soil_NOx_sea_salt_aerosols_and_biogenic_VOCs/9962216/4). National

377 Long-range Transboundary Air Pollution (LRTAP) NO_x emissions are obtained from the European

378 Environment Agency ([https://www.eea.europa.eu/data-and-maps/dashboards/air-pollutant-](https://www.eea.europa.eu/data-and-maps/dashboards/air-pollutant-emissions-data-viewer-5)
 379 [emissions-data-viewer-5](https://www.eea.europa.eu/data-and-maps/dashboards/air-pollutant-emissions-data-viewer-5)). CAMS anthropogenic NO_x and CO₂ emissions are obtained from ECCAD
 380 (<https://permalink.aeris-data.fr/CAMS-GLOB-ANT>). The land use data Land Cover as input data for
 381 our method are downloaded from the Copernicus Global Land Service
 382 (<https://land.copernicus.eu/global/products/lc>).

383

384 References

- 385 Bertram, T. H., Heckel, A., Richter, A., Burrows, J. P. & Cohen, R. C. (2005). Satellite measurements of daily
 386 variations in soil NO_x emissions. *Geophysical Research Letters*, 32(24), <https://doi.org/10.1029/2005gl024640>
 387 Buchhorn, M., Smets, B., Bertels, L., De Roo, B., Lesiv, M., Tsendbazar, N. E., et al. (2020). Copernicus Global
 388 Land Service: Land Cover 100m: version 3 Globe 2015-2019: Product User Manual. Zenodo. Geneva, Switzerland.
 389 Butterbach-Bahl, K., Baggs, E. M., Dannenmann, M., Kiese, R. & Zechmeister-Boltenstern, S. (2013). Nitrous
 390 oxide emissions from soils: how well do we understand the processes and their controls? *Philos Trans R Soc Lond B*
 391 *Biol Sci*, 368(1621), 20130122, <https://doi.org/10.1098/rstb.2013.0122>
 392 Butterbach-Bahl, K., Kahl, M., Mykhaliv, L., Werner, C., Kiese, R. & Li, C. (2009). A European-wide inventory of
 393 soil NO emissions using the biogeochemical models DNDC/Forest-DNDC. *Atmospheric Environment*, 43(7), 1392-
 394 1402, <https://doi.org/10.1016/j.atmosenv.2008.02.008>
 395 Davidson, E. A. & Kingerlee, W. (1997). A global inventory of nitric oxide emissions from soils. *Nutrient Cycling*
 396 *in Agroecosystems*, 48(1), 37-50, <https://doi.org/10.1023/A:1009738715891>
 397 de Laat, J. & van der A, R. (2019). CO₂ Human Emissions: Fingerprints of fossil CO₂ sources. [https://www.che-](https://www.che-project.eu/sites/default/files/2020-01/CHE-D3-4-V1-0.pdf)
 398 [project.eu/sites/default/files/2020-01/CHE-D3-4-V1-0.pdf](https://www.che-project.eu/sites/default/files/2020-01/CHE-D3-4-V1-0.pdf).
 399 Ding, J., Miyazaki, K., van der A, R. J., Mijling, B., Kurokawa, J.-i., Cho, S., et al. (2017b). Intercomparison of
 400 NO_x emission inventories over East Asia. *Atmospheric Chemistry and Physics*, 17(16), 10125-10141,
 401 <https://doi.org/10.5194/acp-17-10125-2017>
 402 Ding, J., van der A, R., Mijling, B., de Laat, J., Eskes, H. & Boersma, K. F. (2022). NO_x emissions in India derived
 403 from OMI satellite observations. *Atmospheric Environment: X*, 14(100174),
 404 <https://doi.org/10.1016/j.aeaoa.2022.100174>
 405 Ding, J., van der A, R. J., Eskes, H. J., Mijling, B., Stavrakou, T., van Geffen, J. H. G. M. & Veefkind, J. P. (2020).
 406 NO_x Emissions Reduction and Rebound in China Due to the COVID-19 Crisis. *Geophysical Research Letters*,
 407 47(19), <https://doi.org/10.1029/2020gl089912>
 408 Ding, J., van der A, R. J., Mijling, B., Jalkanen, J. P., Johansson, L. & Levelt, P. F. (2018). Maritime NO_x
 409 Emissions Over Chinese Seas Derived From Satellite Observations. *Geophysical Research Letters*, 45(4), 2031-
 410 2037, <https://doi.org/10.1002/2017gl076788>
 411 Ding, J., van der A, R. J., Mijling, B. & Levelt, P. F. (2017a). Space-based NO_x emission estimates over remote
 412 regions improved in DECSO. *Atmospheric Measurement Techniques*, 10(3), 925-938, [https://doi.org/10.5194/amt-](https://doi.org/10.5194/amt-10-925-2017)
 413 [10-925-2017](https://doi.org/10.5194/amt-10-925-2017)
 414 Ding, J., van der A, R. J., Mijling, B., Levelt, P. F. & Hao, N. (2015). NO_x emission estimates during the 2014
 415 Youth Olympic Games in Nanjing. *Atmospheric Chemistry and Physics*, 15(16), 9399-9412,
 416 <https://doi.org/10.5194/acp-15-9399-2015>
 417 Douros, J., Eskes, H., van Geffen, J., Boersma, K. F., Compernelle, S., Pinardi, G., et al. (2023). Comparing
 418 Sentinel-5P TROPOMI NO₂ column observations with the CAMS regional air quality ensemble. *Geoscientific*
 419 *Model Development*, 16(2), 509-534, <https://doi.org/10.5194/gmd-16-509-2023>
 420 ECMWF (2023). IFS Documentation CY48R1 - Part VIII: Atmospheric Composition.
 421 <https://www.ecmwf.int/en/elibrary/81374-ifs-documentation-cy48r1-part-viii-atmospheric-composition>.
 422 Eickenscheidt, N. & Brumme, R. (2012). NO_x and N₂O fluxes in a nitrogen-enriched European spruce forest soil
 423 under experimental long-term reduction of nitrogen depositions. *Atmospheric Environment*, 60(51-58),
 424 <https://doi.org/https://doi.org/10.1016/j.atmosenv.2012.06.018>

- 425 Flemming, J., Huijnen, V., Arteta, J., Bechtold, P., Beljaars, A., Blechschmidt, A. M., et al. (2015). Tropospheric
426 chemistry in the Integrated Forecasting System of ECMWF. *Geoscientific Model Development*, 8(4), 975-1003,
427 <https://doi.org/10.5194/gmd-8-975-2015>
- 428 Fortems - Cheiney, A., Broquet, G., Pison, I., Saunois, M., Potier, E., Berchet, A., et al. (2021). Analysis of the
429 Anthropogenic and Biogenic NO_x Emissions Over 2008–2017: Assessment of the Trends in the 30 Most Populated
430 Urban Areas in Europe. *Geophysical Research Letters*, 48(11), <https://doi.org/10.1029/2020gl092206>
- 431 Garcia-Montiel, D. C., Steudler, P. A., Piccolo, M., Neill, C., Melillo, J. & Cerri, C. C. (2003). Nitrogen oxide
432 emissions following wetting of dry soils in forest and pastures in Rondônia, Brazil. *Biogeochemistry*, 64(3), 319-
433 336, <https://doi.org/10.1023/A:1024968802018>
- 434 Hall, S. J. & Matson, P. A. (1999). Nitrogen oxide emissions after nitrogen additions in tropical forests. *Nature*,
435 400(6740), 152-155, <https://doi.org/10.1038/22094>
- 436 Hall, S. J., Matson, P. A. & Roth, P. M. (1996). NO_x EMISSIONS FROM SOIL: Implications for Air Quality
437 Modeling in Agricultural Regions. *Annual Review of Energy and the Environment*, 21(1), 311-346,
438 <https://doi.org/10.1146/annurev.energy.21.1.311>
- 439 Hickman, J. E., Kaya, B., Kebede, A., Kandji, S., Fitch, L., Neill, C., et al. (2021). Little Effect of Land Use on N₂O
440 and NO Emission Pulses Following Rewetting of Dry Soils Across Seasonally Dry sub - Saharan Africa. *Journal of*
441 *Geophysical Research: Biogeosciences*, 126(1), <https://doi.org/10.1029/2020jg005742>
- 442 Huber, D. E., Steiner, A. L. & Kort, E. A. (2020). Daily Cropland Soil NO_x Emissions Identified by TROPOMI
443 and SMAP. *Geophysical Research Letters*, 47(22), e2020GL089949, <https://doi.org/10.1029/2020GL089949>
- 444 Hudman, R. C., Moore, N. E., Mebust, A. K., Martin, R. V., Russell, A. R., Valin, L. C. & Cohen, R. C. (2012).
445 Steps towards a mechanistic model of global soil nitric oxide emissions: implementation and space based-
446 constraints. *Atmospheric Chemistry and Physics*, 12(16), 7779-7795, <https://doi.org/10.5194/acp-12-7779-2012>
- 447 Hui, K., Yuan, Y., Xi, B. & Tan, W. (2023). A review of the factors affecting the emission of the ozone chemical
448 precursors VOCs and NO_x from the soil. *Environment International*, 172(107799),
449 <https://doi.org/10.1016/j.envint.2023.107799>
- 450 Huijnen, V., Pozzer, A., Arteta, J., Brasseur, G., Bouarar, I., Chabrilat, S., et al. (2019). Quantifying uncertainties
451 due to chemistry modelling – evaluation of tropospheric composition simulations in the CAMS model (cycle 43R1).
452 *Geoscientific Model Development*, 12(4), 1725-1752, <https://doi.org/10.5194/gmd-12-1725-2019>
- 453 Keller, C. A., Long, M. S., Yantosca, R. M., Da Silva, A. M., Pawson, S. & Jacob, D. J. (2014). HEMCO v1.0: a
454 versatile, ESMF-compliant component for calculating emissions in atmospheric models. *Geoscientific Model*
455 *Development*, 7(4), 1409-1417, <https://doi.org/10.5194/gmd-7-1409-2014>
- 456 Koehler, B., Corre, M. D., Veldkamp, E., Wullaert, H. & Wright, S. J. (2009). Immediate and long-term nitrogen
457 oxide emissions from tropical forest soils exposed to elevated nitrogen input. *Global Change Biology*, 15(8), 2049-
458 2066, <https://doi.org/https://doi.org/10.1111/j.1365-2486.2008.01826.x>
- 459 Li, H., Zheng, B., Ciais, P., Boersma, K. F., Riess, T. C. V. W., Martin, R. V., et al. (2023). Satellite reveals a steep
460 decline in China's CO₂ emissions in early 2022. *Science Advances*, 9(29), eadg7429,
461 <https://doi.org/doi:10.1126/sciadv.adg7429>
- 462 Lin, J. T. (2012). Satellite constraint for emissions of nitrogen oxides from anthropogenic, lightning and soil sources
463 over East China on a high-resolution grid. *Atmospheric Chemistry and Physics*, 12(6), 2881-2898,
464 <https://doi.org/10.5194/acp-12-2881-2012>
- 465 Liu, S., Lin, F., Wu, S., Ji, C., Sun, Y., Jin, Y., et al. (2017). A meta-analysis of fertilizer-induced soil NO and
466 combined NO+N₂O emissions. *Glob Chang Biol*, 23(6), 2520-2532, <https://doi.org/10.1111/gcb.13485>
- 467 Lu, X., Ye, X., Zhou, M., Zhao, Y., Weng, H., Kong, H., et al. (2021). The underappreciated role of agricultural soil
468 nitrogen oxide emissions in ozone pollution regulation in North China. *Nat Commun*, 12(1), 5021,
469 <https://doi.org/10.1038/s41467-021-25147-9>
- 470 Medinets, S., Skiba, U., Rennenberg, H. & Butterbach-Bahl, K. (2015). A review of soil NO transformation:
471 Associated processes and possible physiological significance on organisms. *Soil Biology and Biochemistry*, 80(92-
472 117, <https://doi.org/10.1016/j.soilbio.2014.09.025>
- 473 Menut, L., Bessagnet, B., Briant, R., Cholakian, A., Couvidat, F., Mailler, S., et al. (2021). The CHIMERE v2020r1
474 online chemistry-transport model. *Geoscientific Model Development*, 14(11), 6781-6811,
475 <https://doi.org/10.5194/gmd-14-6781-2021>
- 476 Mijling, B. & van der A, R. J. (2012). Using daily satellite observations to estimate emissions of short-lived air
477 pollutants on a mesoscopic scale. *Journal of Geophysical Research-Atmospheres*, 117(20),
478 <https://doi.org/10.1029/2012jd017817>
- 479 Miyazaki, K. & Bowman, K. (2023). Predictability of fossil fuel CO₂ from air quality emissions. *Nat Commun*,
480 14(1), 1604, <https://doi.org/10.1038/s41467-023-37264-8>

- 481 Miyazaki, K., Eskes, H. J. & Sudo, K. (2012). Global NO_x emission estimates derived from an assimilation of OMI
482 tropospheric NO₂ columns. *Atmospheric Chemistry and Physics*, 12(5), 2263-2288, [https://doi.org/10.5194/acp-12-](https://doi.org/10.5194/acp-12-2263-2012)
483 [2263-2012](https://doi.org/10.5194/acp-12-2263-2012)
- 484 Molina-Herrera, S., Haas, E., Grote, R., Kiese, R., Klatt, S., Kraus, D., et al. (2017). Importance of soil NO
485 emissions for the total atmospheric NO_x budget of Saxony, Germany. *Atmospheric Environment*, 152(61-76),
486 <https://doi.org/10.1016/j.atmosenv.2016.12.022>
- 487 Pilegaard, K. (2013). Processes regulating nitric oxide emissions from soils. *Philosophical Transactions of the Royal*
488 *Society B: Biological Sciences*, 368(1621), 20130126, <https://doi.org/doi:10.1098/rstb.2013.0126>
- 489 Rafaj, P., Amann, M., Siri, J. & Wuester, H. (2015). Changes in European greenhouse gas and air pollutant
490 emissions 1960–2010: decomposition of determining factors. *Uncertainties in Greenhouse Gas Inventories:*
491 *Expanding Our Perspective*, 27-54,
- 492 Silvern, R. F., Jacob, D. J., Mickley, L. J., Sulprizio, M. P., Travis, K. R., Marais, E. A., et al. (2019). Using satellite
493 observations of tropospheric NO₂ columns to infer long-term trends in US NO_x emissions: the importance of
494 accounting for the free tropospheric NO₂ background. *Atmospheric Chemistry and Physics*, 19(13), 8863-8878,
495 <https://doi.org/10.5194/acp-19-8863-2019>
- 496 Simpson, D. & Darras, S. (2021). Global soil NO emissions for Atmospheric Chemical Transport Modelling:
497 CAMS-GLOB-SOIL v2.2. *Earth System Science Data Discussions*, 2021(1-35), [https://doi.org/10.5194/essd-2021-](https://doi.org/10.5194/essd-2021-221)
498 [221](https://doi.org/10.5194/essd-2021-221)
- 499 Skalska, K., Miller, J. S. & Ledakowicz, S. (2010). Trends in NO(x) abatement: a review. *Sci Total Environ*,
500 408(19), 3976-3989, <https://doi.org/10.1016/j.scitotenv.2010.06.001>
- 501 Skiba, U., Medinets, S., Cardenas, L. M., Carnell, E. J., Hutchings, N. & Amon, B. (2020). Assessing the
502 contribution of soil NO_x emissions to European atmospheric pollution. *Environmental Research Letters*,
503 <https://doi.org/10.1088/1748-9326/abd2f2>
- 504 Song, L., Drewer, J., Zhu, B., Zhou, M., Cowan, N., Levy, P. & Skiba, U. (2020). The impact of atmospheric N
505 deposition and N fertilizer type on soil nitric oxide and nitrous oxide fluxes from agricultural and forest Eutric
506 Regosols. *Biology and Fertility of Soils*, 56(7), 1077-1090, <https://doi.org/10.1007/s00374-020-01485-6>
- 507 Soulie, A., Granier, C., Darras, S., Zilbermann, N., Doumbia, T., Guevara, M., et al. (2023). Global Anthropogenic
508 Emissions (CAMS-GLOB-ANT) for the Copernicus Atmosphere Monitoring Service Simulations of Air Quality
509 Forecasts and Reanalyses. *Earth System Science Data Discussions*, 2023(1-45), [https://doi.org/10.5194/essd-2023-](https://doi.org/10.5194/essd-2023-306)
510 [306](https://doi.org/10.5194/essd-2023-306)
- 511 Valente, R. J. & Thornton, F. C. (1993). Emissions of NO from soil at a rural site in central Tennessee. *Journal of*
512 *Geophysical Research: Atmospheres*, 98(D9), 16745-16753, <https://doi.org/https://doi.org/10.1029/93JD01417>
- 513 van der A, R. J., de Laat, A. T. J., Ding, J. & Eskes, H. J. (2020). Connecting the dots: NO_x emissions along a West
514 Siberian natural gas pipeline. *npj Climate and Atmospheric Science*, 3(1), [https://doi.org/10.1038/s41612-020-0119-](https://doi.org/10.1038/s41612-020-0119-z)
515 [z](https://doi.org/10.1038/s41612-020-0119-z)
- 516 van der A, R. J., Mijling, B., Ding, J., Koukouli, M. E., Liu, F., Li, Q., et al. (2017). Cleaning up the air:
517 effectiveness of air quality policy for SO₂ and NO_x emissions in China. *Atmospheric Chemistry and Physics*, 17(3),
518 1775-1789, <https://doi.org/10.5194/acp-17-1775-2017>
- 519 Venterea, R. T., Groffman, P. M., Verchot, L. V., Magill, A. H., Aber, J. D. & Steudler, P. A. (2003). Nitrogen
520 oxide gas emissions from temperate forest soils receiving long-term nitrogen inputs. *Global Change Biology*, 9(3),
521 346-357, <https://doi.org/https://doi.org/10.1046/j.1365-2486.2003.00591.x>
- 522 Verchot, L. V., Davidson, E. A., Cattânio, H., Ackerman, I. L., Erickson, H. E. & Keller, M. (1999). Land use
523 change and biogeochemical controls of nitrogen oxide emissions from soils in eastern Amazonia. *Global*
524 *Biogeochemical Cycles*, 13(1), 31-46, <https://doi.org/https://doi.org/10.1029/1998GB900019>
- 525 Vinken, G. C. M., Boersma, K. F., Maasakkers, J. D., Adon, M. & Martin, R. V. (2014). Worldwide biogenic soil
526 NO_x emissions inferred from OMI NO₂ observations. *Atmospheric Chemistry and Physics*, 14(18), 10363-10381,
527 <https://doi.org/10.5194/acp-14-10363-2014>
- 528 Wang, R., Bei, N., Wu, J., Li, X., Liu, S., Yu, J., et al. (2022). Cropland nitrogen dioxide emissions and effects on
529 the ozone pollution in the North China plain. *Environmental Pollution*, 294(118617),
530 <https://doi.org/https://doi.org/10.1016/j.envpol.2021.118617>
- 531 Weng, H., Lin, J., Martin, R., Millet, D. B., Jaegle, L., Ridley, D., et al. (2020). Global high-resolution emissions of
532 soil NO_x, sea salt aerosols, and biogenic volatile organic compounds. *Sci Data*, 7(1), 148,
533 <https://doi.org/10.1038/s41597-020-0488-5>
- 534 Yan, X., Ohara, T. & Akimoto, H. (2005). Statistical modeling of global soil NO_x emissions. *Global Biogeochemical*
535 *Cycles*, 19(3), <https://doi.org/10.1029/2004gb002276>

536 Yienger, J. J. & Levy II, H. (1995). Empirical model of global soil-biogenic NO_x emissions. *Journal of Geophysical*
537 *Research: Atmospheres*, 100(D6), 11447-11464, <https://doi.org/https://doi.org/10.1029/95JD00370>
538 Zhang, R., Tie, X. & Bond, D. W. (2003). Impacts of anthropogenic and natural NO_x sources over the U.S. on
539 tropospheric chemistry. *Proceedings of the National Academy of Sciences*, 100(4), 1505-1509,
540 <https://doi.org/doi:10.1073/pnas.252763799>
541 Zheng, B., Geng, G. N., Ciais, P., Davis, S. J., Martin, R. V., Meng, J., et al. (2020). Satellite-based estimates of
542 decline and rebound in China's CO₂ emissions during COVID-19 pandemic. *Science Advances*, 6(49),
543 <https://doi.org/10.1126/sciadv.abd4998>
544 Zörner, J., Penning de Vries, M., Beirle, S., Sihler, H., Veres, P. R., Williams, J. & Wagner, T. (2016). Multi-
545 satellite sensor study on precipitation-induced emission pulses of NO_x from soils in semi-arid ecosystems.
546 *Atmospheric Chemistry and Physics*, 16(14), 9457-9487, <https://doi.org/10.5194/acp-16-9457-2016>
547